Optics Letters

Coupled-mode induced transparency in a bottle whispering-gallery-mode resonator

Yue Wang,[1,2] Kun Zhang,[1,2] Song Zhou,[1,2] Yi-Hui Wu,[1,*] Ming-Bo Chi,[1,2] and Peng Hao[1]

[1]State Key Laboratory of Applied Optics, Changchun Institute of Optics, Fine Mechanics and Physics, Chinese Academy of Sciences, Changchun 130033, China
[2]University of Chinese Academy of Sciences, Beijing 100039, China
*Corresponding author: yihuiwu@ciomp.ac.cn

Received 25 January 2016; revised 13 March 2016; accepted 13 March 2016; posted 15 March 2016 (Doc. ID 258159); published 14 April 2016

Whispering-gallery-mode (WGM) optical resonators are ideal systems for achieving electromagnetically induced transparency-like phenomenon. Here, we experimentally demonstrate that one or more transparent windows can be achieved with coupled-mode induced transparency (CMIT) in a single bottle WGM resonator due to the bottle's dense mode spectra and tunable resonant frequencies. This device offers an approach for multi-channel all-optical switching devices and sensitivity-enhanced WGM-based sensors.

OCIS codes: (140.3948) Microcavity devices; (230.3990) Micro-optical devices; (280.4788) Optical sensing and sensors.

http://dx.doi.org/10.1364/OL.41.001825

An electromagnetically induced transparency-like effect in optical resonant systems, i.e., showing one or more transparent windows in the transmission spectrum, has been intensively exploited due to its potential applications in all-optical switching and quantum information processing [1–8]. This phenomenon can be apprehended as destructive interference between different optical paths. Whispering-gallery-mode (WGM) resonators are good candidates for this effect because of several available physical mechanisms [9–17]. Among them, coupled-mode induced transparency (CMIT) is the easiest to achieve because it involves no other modes besides optical modes, such as a mechanical mode in optomechanically induced transparency or an acoustic mode in Brillouin scattering induced transparency [11–13]. To achieve CMIT, two or more resonant modes with close resonant frequencies should be simultaneously excited. There are two approaches: one is to excite different radial modes in a single WGM resonator, and the other is to use a sequence of resonators in which each resonator contributes one mode [6,7,14–16]. However, the former method is constrained by the mode density of a resonator and is always assisted by a tuning method to shift the resonant frequency. In addition, only a single transparent window is reported. Although the latter method is able to achieve multiple transparent windows, it strictly requires both the frequency tuning of each mode and high-precision micro-nano fabrication technique.

Among all sorts of WGM resonators, the bottle shape has been intensively investigated in light-matter interaction and sensing, owing to its ultra-dense mode spectra and its tunable resonant frequencies [18–23]. These two characteristics make a bottle resonator suitable for CMIT, but it has not been reported. In this Letter, we first demonstrated theoretically that CMIT can be easily attained in a single bottle resonator; then, by exciting different radial modes, we observed an experimentally tunable CMIT effect with both one and two transparent windows in a bottle-fiber coupling system. This device could pave the way toward practical applications in multi-channel all-optical switching devices and sensitivity-enhanced WGM-based sensors [7,8,24–26].

The bottle configuration could be depicted as a truncated harmonic-oscillator profile $R(z) = R_0[1-1/2(\Delta k z)^2]$, where z is the resonator axis direction, R_0 is the radius at $z = 0$, and Δk is the curvature of the resonator profile. Its resonant mode is characterized by radial, azimuthal, and axial mode numbers; it is expressed in the form of (n, m, q). Considering the polarization effect, its resonant frequency $\nu = c/(\lambda n_0)$, with resonant wavelength expressed as [27]

$$\lambda_{nmq} = 2\pi n_0 \left[\left(\frac{U_{nm}}{R_0}\right)^2 + \left(q+\frac{1}{2}\right)\frac{2U_{nm}\Delta k}{R_0}\right]^{-1/2}, \quad (1)$$

where n_0 is the resonator refractive index, c is the light speed in vacuum, and

$$U_{nm} = m + \alpha_n\left(\frac{m}{2}\right)^{1/3} - \frac{p}{(n^2-1)^{1/2}} + \left(\frac{3}{20}\right)\alpha_n^2\left(\frac{m}{2}\right)^{-1/3}. \quad (2)$$

Here, α_n is the nth root of the Airy function, $p = n_0$ for transverse electric mode, and $p = 1/n_0$ for the transverse magnetic mode. In one radial mode family, its resonant frequencies are discrete and are separated by the axial free spectrum range (FSR), $\mathrm{FSR}_q \approx c\Delta k/(2\pi n_0)$. In practice, modes of close-by axial and nonsequential azimuthal order could be excited together for a bottle-fiber coupling system; thus, the bottle exhibits dense mode spectra. Furthermore, the radial modes with $n \leq 3$ can be excited simultaneously using one taper fiber [27]. For instance, Fig. 1 shows the mode spectra of a bottle resonator with $\Delta k = 0.0019\ \mu\mathrm{m}^{-1}$ and $R_0 = 70\ \mu\mathrm{m}$. It is found that

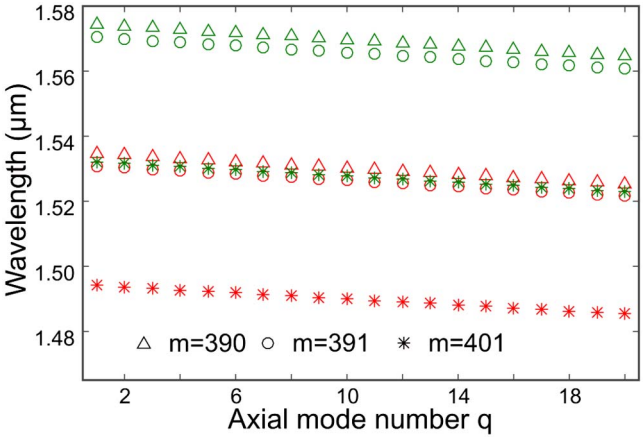

Fig. 1. Mode spectra of a bottle resonator with $R_0 = 70$ μm and $\Delta k = 0.0019$ μm^{-1}. The green and red colors of each signal denote $n = 1$ and $n = 2$ radial modes, respectively.

around 1553.5 nm, the frequency of mode (1, 401, q) locates between two consecutive azimuthal modes (2, 391, q) and (2, 390, q). This means that different radial mode families are intersecting, i.e., the nearest resonance of $n = 1$ mode could be $n = 2$ or $n = 3$ mode, which further increases the mode density. This feature holds for different axial mode numbers, i.e., different positions along the axial direction. Therefore, frequency overlapping in a bottle resonator can be easily achievable.

Bottle WGM resonator was fabricated by fusing a standard telecom fiber ($R_0 = 70$ μm) with a fiber fusion splicer. Using different numbers of arc discharges, bottles with curvature ranging from 0.01 to 0.0019 μm^{-1} were produced. Because the smaller curvature brings the denser mode spectra, a bottle of $\Delta k = 0.0019$ μm^{-1} is utilized to achieve mode coupling. The experimental setup is presented in Fig. 2(a). The input light, after passing a fiber polarization controller, excites the bottle resonant mode evanescently with a taper fiber. The output is monitored by an oscilloscope linked with a photo detector. To excite different radial modes effectively, the tapered region of the taper fiber is maintained in physical contact with the bottle surface [28]. A piezoelectric transducer (PZT) is used to tune the resonant frequency by stretching the bottle.

The resonant frequencies are not intrinsically overlapped with each other in most cases. This frequency difference can be compensated by tuning the bottle's radius with external strain due to different radial mode responses, i.e., the resonant wavelength of low-order radial mode shifts blue at a larger rate than high-order mode [15]. Figure 2(b) selects three modes termed M1, M2, and M3 to determine their response characteristics in our system. It is evident that the resonance peaks shift linearly with the increase of voltage, as shown in Fig. 2(c). M2 and M3 have nearly the same response rate of 0.15 GHz/V, while M1 has a larger response rate of 0.3 GHz/V. Thus, it is predicted that M1 belongs to low-order radial modes, and M2 and M3 are the same high-order radial modes. Notably, the frequency difference (3 GHz) between M2 and M3 is far less than the axial FSR (62.7 GHz). This is because the radius of the taper fiber must be around 1.65 μm to effectively excite the resonant mode of a bottle ($R_0 = 70$ μm). In this case, resonant modes with the same radial mode number, but different azimuthal and axial mode numbers, can be excited together because of their

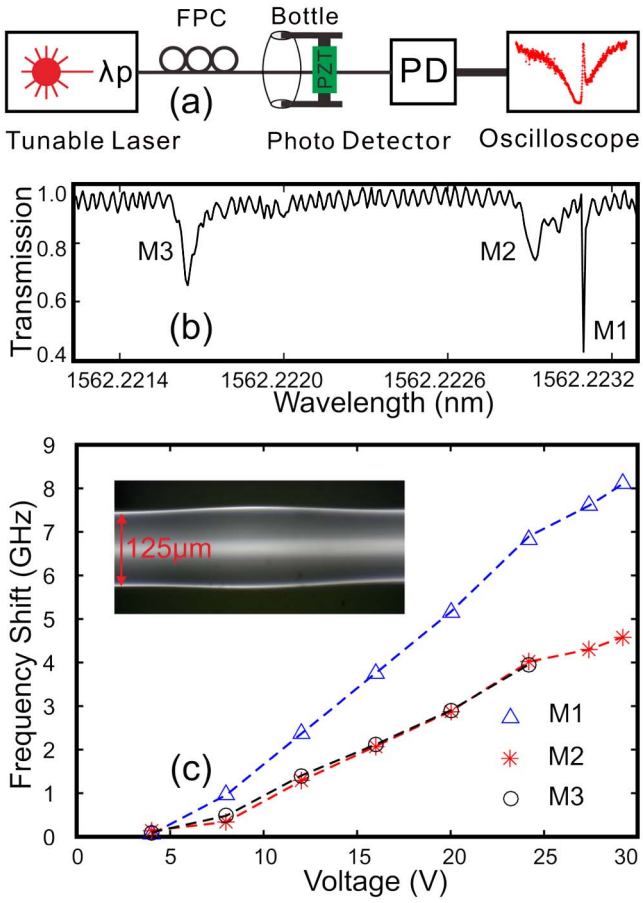

Fig. 2. (a) Schematic of the experimental setup. FPC, fiber polarization controller; PZT, piezoelectric transducer. (b) Three resonant modes selected to identify the response characteristics of different radial modes. (c) Resonant frequency shift responses of different radial modes. The inset is an optical picture of the bottle WGM resonator used in the experiment, $\Delta k = 0.0019$ μm^{-1} and $R_0 = 70$ μm. The experimental data of M3 are less because it is tuned out of the sweeping range.

close resonant frequencies and propagation constants [27,28]. Therefore, the tuning range of a resonance peak as large as one axial FSR [19] can facilitate the frequency overlapping between two separated modes.

In theory, CMIT can be apprehended as destructive interference between different optical pathways and can be explained by the coupled-mode equations introduced in [17] as

$$\frac{d\alpha_A}{dt} = -i\Delta\omega_A\alpha_A - \frac{\gamma_A + \kappa_A}{2}\alpha_A - \sum_i g_{Ai}\alpha_i + \sqrt{\kappa_A}\alpha_{\text{in}}\cos\theta,$$
$$\frac{d\alpha_i}{dt} = -i\Delta\omega_i\alpha_i - \frac{\gamma_i + \kappa_i}{2}\alpha_i - g_{Ai}\alpha_A + \sqrt{\kappa_i}\alpha_{\text{in}}\cos(\varphi_i - \theta), \quad (3)$$

where i denotes integer. $i + 1$ coupled modes result in i transparent windows in the transmission spectrum, and each window corresponds to a relatively high Q-factor mode. The frequency difference between two adjacent window modes is assumed to be larger than their linewidths; thus, there is no coupling between them. As shown in Fig. 3, α_A denotes a low Q-factor mode termed valley mode; α_i denotes a window

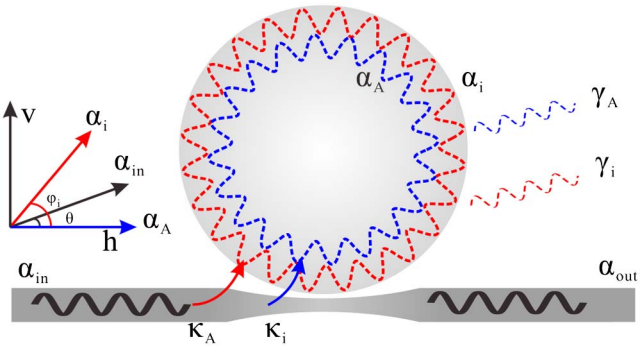

Fig. 3. Schematic of the coupled modes in the resonator. The red and blue lines denote different radial modes, i.e., a window mode and a valley mode, respectively. In our experimental results, the valley (low Q-factor) mode is the high-order radial mode, but this does not hold for all situations because the loaded Q-factor mainly depends on the external coupling rate.

resonant mode; and $\Delta\omega_A$ and $\Delta\omega_i$ are their frequency deviations from the incident light, respectively. κ_A (κ_i) is the external coupling rate of α_A (α_i); γ_A (γ_i) is its intrinsic loss rate; and g_{Ai} is the coupling strength between α_A and α_i, determined by $g_{Ai} = (\kappa_A \cdot \kappa_i)^{1/2} \cdot \cos\psi_i/2$. α_{in} is the input electric field; and θ and ψ_i are the polarization orientations of modes α_{in} and α_i relative to mode α_A, respectively. When solved in steady state, the transmission spectrum can be derived as

$$T = \frac{1}{|\alpha_{\text{in}}|^2}\left[\left|\alpha_{\text{in}}\cos\theta + \sqrt{\kappa_A}\alpha_A + \sum_i \sqrt{\kappa_i}\alpha_i \cos\varphi_i\right|^2 + \left|\alpha_{\text{in}}\sin\theta + \sum_i \sqrt{\kappa_i}\alpha_i \sin\varphi_i\right|^2\right]. \quad (4)$$

Experimentally, by keeping the tapered region of the fiber in contact with the bottle, tens of micrometers away from the equator and sweeping the incident wavelength, we found two close resonant modes A and B, as shown in Fig. 4(a). They are separated by about 3 GHz, and their Q-factors are approximated to be 2×10^5 and 9×10^6, respectively. The two resonant frequencies were then tuned by stretching the bottle with the PZT, and the window mode B generally swept across the valley mode A as presented in Figs. 4(b)–4(d), showing tunable CMIT phenomenon. The experimental CMIT is in accord with the theoretical results. The mismatch between the fitting and the experiment is attributed to the involvement of other low Q-factor modes and the experimental environment. From the fittings, we find that the coupling condition for each mode changes slightly during stretching, but the window mode is always overcoupled ($\kappa_B > \gamma_B$), and the valley mode is undercoupled ($\kappa_A < \gamma_A$). This is consistent with the theoretical results in [14,29]. From the perspective of interference, the transmission power consists of three parts, i.e., the power transmitting the tapered fiber directly and the power coupling out of the two WGMs. We assume that interaction between the two coupled WGMs changes the coupling condition of the valley mode; hence, it changes the transmission power [30]. In this situation, the undercoupled valley mode is tuned to be overcoupled near the central frequency of mode B. Power coupled out of the resonator becomes the major component of the transmission power; then we have an increased transmission power.

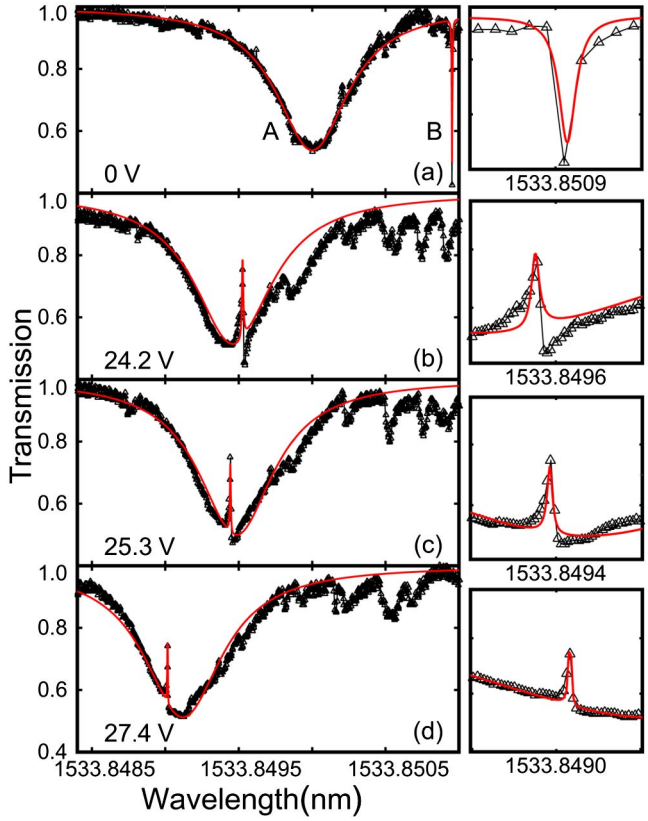

Fig. 4. Experimental CMIT at different voltages. The red line is the theoretical fitting, and the black triangle is the experimental transmission spectrum. In the fitting, (γ_A, κ_A, γ_B, κ_B, θ, ψ_b) were uniquely determined using the weighted least-square method according to experimental results. The fitting parameters used in the fitting are (a) [$\kappa_A(\gamma_A)$, $\kappa_B(\gamma_B)$] = [0.2 (1.3), and 0.01 (0.002) GHz; (b) [$\kappa_A(\gamma_A)$, $\kappa_B(\gamma_B)$] = [0.26 (1.36), and 0.03 (0.002)] GHz; (c) [$\kappa_A(\gamma_A)$, $\kappa_B(\gamma_B)$] = [0.26 (1.3), and 0.02 (0.001)] GHz; and (d) [$\kappa_A(\gamma_A)$, $\kappa_B(\gamma_B)$] = [0.26 (1.36), 0.008 (0.0002)] GHz, and $\theta = \pi/10$, $\psi_b = \pi/9$. In the experiment, the FPC was fixed to a certain polarization. Zoom-ins of each window mode are shown on the right. The appearance of a Fano-shaped mode is attributed to the slight changes in the coupling conditions.

At this moment, a new mode distribution is built, and the frequency can be regarded as the eigenfrequency of the bottle-fiber coupling system [31,32]. Moreover, it is noted that the tuning range of the transparent window is limited by the linewidth of the valley mode. To achieve a larger tuning range, it is suggested to involve another tuning method, in which the coupled two modes respond at the same rate, like thermal control [6,33].

In addition, as implied by Fig. 4, there are several modes around the coupled modes A and B. Thus, it is anticipated to observe two or more transparent windows within one valley mode in a single bottle resonator experimentally. Here, as shown in Fig. 5, modes B and C, separated by about 24.5 MHz, exhibit two windows in mode A. The loaded Q-factors of the two window modes are approximated to be 3×10^7 for mode B and 4×10^6 for mode C, respectively. These are two orders of magnitude larger than the Q-factor achieved in coupled ring resonators [6]. By fitting the experimental results, we find that all three modes are overcoupled, which enables the coupling system to be robust against the external disturbance. In this situation, interference

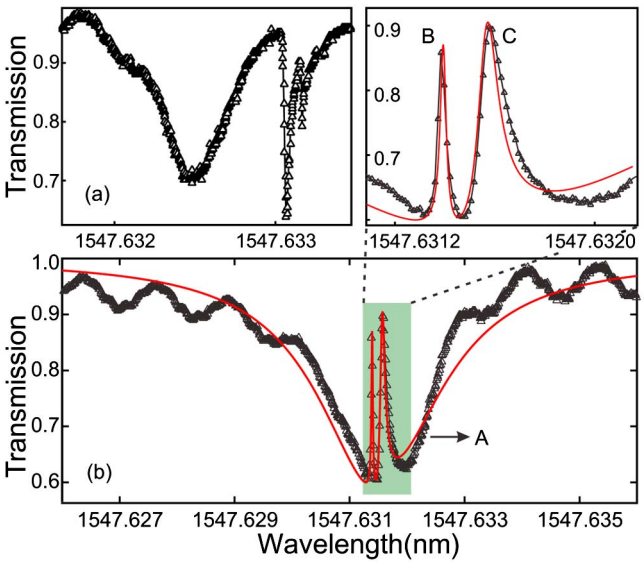

Fig. 5. (a) Three modes for mode coupling. (b) Experimental CMIT with two transparent windows. The red line is the theoretical fitting, and the black triangle is the experimental transmission spectrum. Mode A is the valley mode, and modes B and C are two window modes. The fitting parameters used in the fitting are $[\kappa_A(\gamma_A), \kappa_B(\gamma_B), \kappa_C(\gamma_C)] = [0.24\ (0.046), 0.0043\ (0.0026), 0.045\ (0.001)]$ GHz, and $[\theta, \psi_b, \psi_c] = [\pi/40, \pi/9, \pi/10]$. The inset is the closeup of the two window modes B and C.

enhances the overcoupling condition of the valley mode and, hence, results in an increased transmission power [29]. Furthermore, modes B and C shift at almost the same rate when stretching, which means that they belong to the same radial mode family. To tune the frequency difference between them, each frequency should be tuned individually. This can be facilitated by modulating the refractive index of each mode distribution as introduced in [34]. Finally, achieving CMIT with multiple windows in a single bottle resonator significantly reduces the requirement on micro-nano fabrication technique in producing a coupled resonator system. To achieve CMIT with three or more window modes in a single resonator, however, remains challenging. Mode identification of the coupled modes and polarization effect will be examined in our further work.

In summary, we have theoretically demonstrated that a bottle WGM resonator is suitable for CMIT phenomenon. Because it has ultra-dense mode spectra and frequency, overlapping can be achieved in many positions along the axis direction. In addition, the demonstration is verified by the tunable CMIT with one window and two windows experimentally. Such feasibility and selectivity make the bottle resonator a practical element in applications, such as multi-channel all-optical switching devices and sensitivity-enhanced WGM-based sensors.

Funding. National High Technology Research and Development Program of China (2015AA042402).

Acknowledgment. The authors thank Zhiyong Wu, Shijie Gao, Jiabin Wu, DanDan Ge, Quanlong Wang in CIOMP, and Chang Chen in UIUC. The authors are also grateful to the anonymous reviewers.

REFERENCES

1. R. W. Boyd, *Nonlinear Optics*, 3rd ed. (Academic, 2010), p. 185.
2. M. D. Lukin and A. Imamoğlu, Nature **413**, 273 (2001).
3. D. D. Smith, H. Chang, K. A. Fuller, A. T. Rosenberger, and R. W. Boyd, Phys. Rev. A **69**, 063804 (2004).
4. X.-D. Yang, M.-B. Yu, D.-L. Kwong, and C.-W. Wong, Phys. Rev. Lett. **102**, 173902 (2009).
5. B. D. Clader, R. M. Camacho, and B. C. Jacobs, Opt. Express **21**, 6169 (2013).
6. M. Mancinelli, P. Bettotti, J. M. Fedeli, and L. Pavesi, Opt. Express **20**, 23856 (2012).
7. Y.-F. Xiao, X.-B. Zou, W. Jiang, Y.-L. Chen, and G.-C. Guo, Phys. Rev. A **75**, 063833 (2007).
8. Z.-H. He, H.-J. Li, S.-P. Zhan, B.-X. Li, Z.-Q. Chen, and H. Xu, Sci. Rep. **5**, 15837 (2015).
9. C. Zheng, X.-S. Jiang, S.-Y. Hua, L. Chang, G.-Y. Li, H.-B. Fan, and M. Xiao, Opt. Express **20**, 18319 (2011).
10. C.-H. Dong, C.-L. Zou, Y.-F. Xiao, J.-M. Cui, Z.-F. Han, and G.-C. Guo, J. Phys. B **42**, 215401 (2009).
11. J.-H. Kim, M. C. Kuzyk, K.-W. Han, H.-L. Wang, and G. Bahl, Nat. Phys. **11**, 275 (2015).
12. C.-H. Dong, Z. Shen, C.-L. Zou, Y.-L. Zhang, W. Fu, and G.-C. Guo, Nat. Commun. **6**, 6193 (2015).
13. S. Weis, R. Rivière, S. Deléglise, E. Gavartin, O. Arcizet, A. Schliesser, and T. J. Kippenberg, Science **330**, 1520 (2010).
14. Y.-F. Xiao, L.-N. He, J.-G. Zhu, and L. Yang, Appl. Phys. Lett. **94**, 231115 (2009).
15. Y. Yang, S. Saurabh, J. Ward, and S. N. Chormaic, Opt. Lett. **40**, 1834 (2015).
16. A. Naweed, G. Farca, S. I. Shopova, and A. T. Rosenberger, Phys. Rev. A **71**, 043804 (2005).
17. B.-B. Li, Y.-F. Xiao, C.-L. Zou, Y.-C. Liu, X.-F. Jiang, Y.-L. Chen, Y. Li, and Q.-H. Gong, Appl. Phys. Lett. **98**, 021116 (2011).
18. M. Sumetsky, Opt. Lett. **29**, 8 (2004).
19. M. Pöllinger, D. O'shea, F. Warken, and A. Rauschenbeutel, Phys. Rev. Lett. **103**, 053901 (2009).
20. D. O'shea, C. Junge, M. Pöllinger, A. Vogler, and A. Rauschenbeutel, Appl. Phys. B **105**, 129 (2011).
21. M. Sumetsky, Phys. Rev. Lett. **111**, 163901 (2013).
22. D. O'shea, C. Junge, J. Volz, and A. Rauschenbeutel, Phys. Rev. Lett. **111**, 193601 (2013).
23. K. H. Kim, G. Bahl, W. Lee, J. Liu, M. Tomes, X. Fan, and T. Carmon, Light: Sci. Appl. **2**, e110 (2013).
24. Y.-F. Xiao, V. Gaddam, and L. Yang, Opt. Express **16**, 12538 (2008).
25. X.-Y. Zhou, L. Zhang, A. M. Armani, D.-H. Zhang, X.-X. Duan, J. Liu, H. Zhang, and W. Pang, IEEE J. Sel. Top. Quantum Electron. **20**, 5200110 (2014).
26. M. R. Foreman, J. D. Swaim, and F. Vollmer, Adv. Opt. Photon **7**, 168 (2015).
27. G. S. Murugan, M. N. Petrovich, Y. Jung, J. S. Wilkinson, and M. N. Zervas, Opt. Express **19**, 20773 (2011).
28. J. C. Knight, G. Cheung, F. Jacques, and T. A. Birks, Opt. Lett. **22**, 1129 (1997).
29. X.-Y. Zhou, L. Zhang, W. Pang, H. Zhang, Q.-R. Yang, and D.-H. Zhang, New J. Phys. **15**, 103033 (2013).
30. K. Totsuka and M. Tomita, J. Opt. Soc. Am. B **23**, 2194 (2006).
31. T. Carmon, H. G. L. Schwefel, L. Yang, M. Oxborrow, A. D. Stone, and K. J. Vahala, Phys. Rev. Lett. **100**, 103905 (2008).
32. F. Li, J. F. Manceau, Y.-H. Wu, and F. Bastien, Appl. Phys. Lett. **93**, 174101 (2008).
33. K. Totsuka, N. Kobayashi, and M. Tomita, Phys. Rev. Lett. **98**, 213904 (2007).
34. Q.-L. Wang, Y. Wang, Z. Guo, J.-F. Wu, and Y.-H. Wu, Opt. Lett. **40**, 1607 (2015).